

# Open Research Online

---

The Open University's repository of research publications and other research outputs

## New Ar-Ar ages of southern Indian kimberlites and a lamproite and their geochemical evolution

### Journal Item

#### How to cite:

Osborne, Ian; Sherlock, Sarah; Anand, Mahesh and Argles, Tom (2011). New Ar-Ar ages of southern Indian kimberlites and a lamproite and their geochemical evolution. *Precambrian Research*, 189(1-2) pp. 91–103.

For guidance on citations see [FAQs](#).

© 2011 Elsevier B.V.



<https://creativecommons.org/licenses/by-nc-nd/4.0/>

Version: Accepted Manuscript

Link(s) to article on publisher's website:

<http://dx.doi.org/doi:10.1016/j.precamres.2011.05.004>

---

Copyright and Moral Rights for the articles on this site are retained by the individual authors and/or other copyright owners. For more information on Open Research Online's data [policy](#) on reuse of materials please consult the policies page.

---

[oro.open.ac.uk](http://oro.open.ac.uk)

# New Ar-Ar ages of southern Indian kimberlites and a lamproite and their geochemical evolution

Ian Osborne<sup>a,\*</sup>, Sarah Sherlock<sup>a</sup>, Mahesh Anand<sup>a,b</sup>, Tom Argles<sup>a</sup>

<sup>a</sup> *Department of Earth and Environmental Sciences, CEPSAR, The Open University,  
Walton Hall, Milton Keynes MK7 6AA, UK*

<sup>b</sup> *Department of Mineralogy, The Natural History Museum, Cromwell Road, London,  
SW7 5BD, UK*

## Abstract

The kimberlites and lamproites of southern India are thought to have formed in the most prolific known period of Precambrian ultramafic/ultrapotassic magmatism at around 1100 Ma. This study reports new age data for southern Indian ultrapotassic rocks (kimberlites and lamproites), a controversial topic due to the wide range of published age data and disagreements over the reliability of previously published ages. In this study we obtained new high-precision Ar-Ar data that better constrain the ages of southern Indian ultrapotassic rocks. Dates from three samples are presented, including two kimberlites from Wajrakarur kimberlite field and one lamproite from the Krishna lamproite field. These age data are then combined with bulk-rock geochemical and Nd isotopic data to provide further constraints on the source region and primary magma composition of southern Indian kimberlites and lamproites. Previously, the Chelima lamproite (ca. 1400 Ma) was considered to be one of the oldest lamproites in the world. However, our age data suggest that at least one lamproite (Pochampalle) was generated in the same region 100 Ma before the Chelima event. The Pochampalle lamproite was emplaced around ~1500 Ma as shown by the Ar-Ar data in this study, roughly 250 Ma before the other Krishna lamproites. It would seem that the Pochampalle lamproite was also derived from an isotopically distinct source region with a lower <sup>143</sup>Nd/<sup>144</sup>Nd ratio than other lamproites in the Krishna field. These findings not only have implications for regional ultramafic/ultrapotassic magmatism, but also demonstrate that the mantle processes for producing lamproitic melts existed earlier than previously thought.

**Keywords:** Kimberlite, Lamproite, Eastern Dharwar Craton, Southern India, Proterozoic,  
Ar-Ar dating

---

\* Corresponding author. Tel.: +44-1908-653023; Fax: +44-1908-655151.

*E-mail address:* I.Osborne@open.ac.uk

35

## 36 **1. Introduction**

37 Kimberlites and lamproites represent ultramafic magmas that travel rapidly from  
38 source regions in the deep mantle (>100 km) to the shallowest crustal levels at speeds  
39 of up to 0.1 to 4.0 ms<sup>-1</sup> (Kelley & Wartho, 2000). In effect, they provide snapshots of  
40 the geochemical and isotopic nature of the deep lithospheric or asthenospheric mantle  
41 at the time of their emplacement. Because their petrogenesis has critical implications  
42 for large-scale processes (e.g. subduction, rifting, mantle plumes, lithospheric  
43 enrichment), accurate determination of their ages is important in order to investigate  
44 the evolution of the deep mantle through time.

45

46 The majority of known kimberlite and lamproite occurrences (>80%) globally are  
47 Mesozoic or Cenozoic in age and are often associated with periods of continental  
48 rifting and formation of ocean basins. For example, Cretaceous kimberlite and related  
49 magmatism in Southern Africa (125-55 Ma) closely follows the opening of the South  
50 Atlantic Ocean, which initiated around 130 Ma ago; similarly the majority of  
51 kimberlites and related ultramafic lamprophyres in Labrador, Quebec, West  
52 Greenland and Scandinavia were emplaced 630-560 Ma ago and linked to the  
53 Eocambrian opening of the Iapetus Ocean (Kumar et al., 2007). Heaman et al. (2003)  
54 indicate a lack of worldwide known kimberlite occurrences between 250 and 360 Ma  
55 that may be linked to relative crustal and mantle stability during the lifetime of the  
56 Gondwanaland supercontinent. It could therefore be proposed that a similar lack of  
57 kimberlite and lamproite occurrences of Proterozoic age is also due to crustal and  
58 mantle stability.

59

60 Proterozoic kimberlite and lamproites are relatively rare by comparison with  
61 Phanerozoic occurrences. The kimberlites and lamproites of southern India are  
62 thought to have formed in the most prolific known period of Precambrian ultramafic  
63 magmatism at around 1100 Ma. Kimberlites, lamproites and related alkalic rocks with  
64 emplacement ages of ~ 1100-1200 Ma have been reported from India, Canada,  
65 Greenland, Australia, Liberia, N. America, Scandinavia and South Africa (Kumar et  
66 al., 2007). Consequently this period of magmatism has been suggested to represent a  
67 global 'mantle event', when mantle conditions must have been favourable for  
68 kimberlite and lamproite emplacement (Skinner et al., 1985).

69

70 The kimberlites and lamproites of India have been proposed to be related to the  
71 formation of the Rodinia supercontinent (Kumar et al., 2007), which existed between  
72 1000 and 750 Ma ago (Dalziel et al., 2000). The supercontinent began to form at ~1  
73 Ga by accretion and collision of fragments produced by breakup of the older  
74 supercontinent, Columbia, which was assembled by global-scale 2.0-1.8 Ga  
75 collisional events (Zhao et al., 2004). Rodinia is thought to have included India,  
76 Australia and many of the present day continents of the southern hemisphere, which  
77 subsequently reorganized to form Gondwana.

78

79 The break-up of Columbia and initial assembly of Rodinia occurred ~1100 Ma ago,  
80 which may have provided favourable conditions for generation and emplacement of  
81 kimberlitic magmas across the Rodinian continent, producing many of the known  
82 Proterozoic kimberlites (~1100 Ma). During the formation of Rodinia ~ 1100 Ma  
83 ago, intracontinental rifting was taking place, resulting in the formation of several  
84 Large Igneous Provinces; e.g., 1109-1086 Ma in Laurentia (Ernst and Buchan, 2001)

and 1112-1102 Ma in the Kalahari Craton (Hanson et al., 2004). Kumar et al. (2007) also proposed an enhanced period of mantle plume activity, approximately 100 Ma prior to the formation of Rodinia.

The petrogenesis of the southern Indian kimberlites is currently still debated and several theories have been put forward. Chalapathi Rao et al. (2004) suggested that they are the result of lithospheric extension during the Mid-Proterozoic. This model proposes a sub-continental lithospheric source that experienced metasomatic enrichment caused by the migration of volatile-rich small fraction melts from the convecting mantle. The model also indicates that the kimberlites are the products of small-degree partial melting of a garnet peridotite mantle source, extensively depleted prior to metasomatic enrichment and subsequent partial melting (Chalapathi Rao et al., 2004). In contrast, Paton et al. (2009) suggested that the southern Indian kimberlites were derived directly from asthenospheric depths. Based on perovskite Sr and bulk-rock Hf and Nd isotopic data, these authors proposed that the asthenospheric component must have originated from within or below the transition zone, and may represent ancient subducted oceanic crust. Kumar et al. (2007) proposed that the southern Indian kimberlites located in the Eastern Dharwar craton (EDC) are likely to be linked to the impingement of a short-lived mantle plume beneath the Dharwar Craton, or that a major change and re-organization of the mantle convection regime occurred at the time of their formation.

There is also debate over whether lamproites are derived from the lithospheric (Davies et al., 2006) or convecting mantle (Murphy et al., 2002). Their complex geochemistry suggests a mantle source region that experienced both depletion and

enrichment. For the Krishna lamproites there are currently three main theories put forward for their formation. Chalapathi Rao et al. (2004) suggested that the source region underwent an extensive initial depletion involving komatiitic type melt extraction, followed by subsequent enrichment by a depleted MORB-type source. Paul et al. (2007) proposed that they were derived from partial melting of a mantle source that was metasomatically enriched in Ti and Fe. This same study also suggested that the lamproites were derived from depths shallower than the garnet stability field and their source regions were shallower than those of the kimberlites in the Eastern Dharwar Craton (EDC). Chakrabarti et al. (2007) maintained that the Krishna lamproites were derived by partial melting of metasomatized subducted Archean komatiite, in a peridotite mantle-source assemblage. In their study, Chakrabarti et al. (2007) argued that the Pb-isotopic signatures (high  $^{207}\text{Pb}$  low  $^{206}\text{Pb}$ ) and superchondritic Nb/Ta ratios in Krishna lamproites ruled out their derivation from a metasomatized sub-continental lithospheric mantle source and instead suggested an Archean crustal component in the source (Chakrabarti et al., 2007).

There are relatively few known kimberlite and lamproite occurrences before ~1100 Ma, e.g., lamproite in Karelia, Russia 2.74 Ga (Sergreev et al., 2007); Kimberlite located in the Guyana Craton, Venezuela age dated at  $1732 \pm 82$  using Rb-Sr chronometry (Nixon et al., 1992). The Proterozoic kimberlites and lamproites of southern India (Fig. 1) therefore provide a rare opportunity to study some of the oldest known occurrences of these rock types.

Previously published age data for the southern Indian kimberlites has been controversial, with different dating techniques showing wide ranges in age, while

several individual pipes remain undated. It has been proposed that the kimberlites in the EDC had a contemporaneous emplacement at around 1.1 Ga (Kumar et al., 2007). The age of the Majhgawan lamproite body ( $1067 \pm 31$  Ma) located 1000 km to the north of the Wajrakarur kimberlite field, fuelled speculation that ultrapotassic, alkaline and mafic magmatism at this time occurred on a greater scale across India. Kumar et al. (2007) suggested that the 1.1 Ga potassic-ultrapotassic and alkaline mafic-magmatism in India was a part of a global geodynamic event as kimberlites and lamproites of similar ages are recognized worldwide in countries such as Australia, Greenland, Liberia, North America, Scandinavia and South Africa.

This study presents robust new ages for the emplacement of some southern Indian kimberlites and lamproites and uses Ar-Ar age dating techniques on phlogopite separates. Our work focuses predominantly on the Krishna lamproites, which in particular lack reliable data to constrain their emplacement age(s). These age data are then combined with geochemical data from the kimberlites and lamproites to provide further constraints on the source region, and primary magma composition, prior to kimberlite and lamproite emplacement. Our new age data for the kimberlites and lamproites also provides insight into the geodynamic evolution of this region.

## **2. The southern Indian kimberlites and lamproites**

The majority of kimberlite and lamproite intrusions in the region occur within the Eastern Dharwar craton (EDC) (Fig.1). Kimberlites crop out to the west of the Cuddapah Basin, while lamproites intrude the basin and its north-eastern margin. Among these are the Krishna lamproites (Fig. 1), which are thought to be some of the

oldest lamproite occurrences globally (Chalapathi Rao et al., 2004), and speculated to be the sources of several of the notable Indian diamonds (Chakrabarti et al., 2007).

The EDC is primarily composed of ancient (>2 Ga), greenschist- to granulite-facies schists and gneisses (Chalapathi Rao et al., 2004). The Eastern Ghat orogeny (1.3-1.6 Ga) affected the EDC, resulting in a narrow, highly deformed granulite-facies belt extending from Chennai to near Kolkota. The ~2.0 Ga old Cuddapah Basin (Anand et al., 2003) covers an area of around 44000 km<sup>2</sup> (Nagaraja Rao et al., 1987) and lies within the EDC. It comprises a 6 to 12 km thick succession of igneous and sedimentary rocks of Early to Late Proterozoic age.

The kimberlites in the EDC predominantly occur in two spatially separated groups: the diamondiferous Wajrakarur kimberlite field (WKF) and the Naryanpet kimberlite field (NKF) (Fig. 2).

The Cuddapah Lamproite Field (CLF) comprises two lamproites - Chelima and Zangamarajupalle. The 30 known lamproites from the Krishna Lamproite Field (KLF) (Fig. 3) occur mainly as dikes and are hosted by early Proterozoic granites of the Peninsular Gneissic Complex of the Dharwar Craton.

### *2.1 Previous age determinations of kimberlites and lamproites in southern India*

All radiometric ages determined for kimberlites and lamproites from this region have yielded Proterozoic ages (see Table 1 and references therein); however, it is vigorously debated whether the southern Indian kimberlites are contemporaneous, or



whether they represent separate magmatic episodes (e.g. Chalapathi Rao et al., 2004; Kumar et al., 2007).

Kumar et al. (2007) argued for a contemporaneous emplacement at around 1.1 Ga for all the kimberlites in the Eastern Dharwar Craton. In contrast, Chalapathi Rao et al (1996, 1999) used their age data (Table 1) to suggest that there were two episodes of Proterozoic mafic potassic magmatic activity in the EDC: one at ca. 1.4 Ga for the NKF and a second at 1.1 Ga for the WKF. However, further age data (Table 1) for the NKF using various techniques (Rb-Sr and U-Pb; Kumar et al 2001, 2007; K-Ca; Gopalan and Kumar, 2008) indicated that the NKF and WKF were both emplaced at ~1100 Ma.

There are few ages for the Indian lamproites, especially for those from EDC (Table 1) and those that are published are considered unreliable because of alteration effects in the kimberlite and lamproites. Only one lamproite from the KLF (Ramannapeta) has been dated previously. Kumar et al. (2001) reported a Rb-Sr age for the Rammanapeta lamproite ( $1224 \pm 14$  Ma), which although contradicts the K-Ar age ( $1384 \pm 18$  Ma) reported by Chalapathi Rao et al. (1996), has been used more frequently to represent the emplacement age of the entire KLF (e.g. Chakrabarti et al., 2007). This is because the possibility that excess Ar in mantle-derived phlogopite causes the older K-Ar ages (as shown by some Siberian and South African kimberlites e.g., Pearson et al., 1995) cannot be ruled out.

For the Chelima lamproite, the ages of Chalapathi Rao et al (1996) and Kumar et al 2001 are in agreement. However, Kumar et al. (2001) suggested that their Rb-Sr ages

for Chelima and Zangamarajupalle were only tentative, as these samples display extensive secondary carbonation, which may have adversely affected the “true” crystallization ages of the lamproites. The K-Ar age reported by Chalapathi et al. (1996) has also been considered unreliable (Kumar et al., 2005) due to the possibility of excess Ar in mantle-derived phlogopite leading to the older K-Ar ages.

From Table 1 and the preceding discussion it is apparent that the recent age determinations provide a compelling argument for contemporaneous kimberlite emplacement in the EDC at around 1100 Ma. However, little reliable data exists for the lamproites from Southern India, and in particular the KLF; the published ages (Table 1) suggest that the kimberlites are not contemporaneous with the older lamproites.

In this study we employed the Ar-Ar method to determine new age data to better constrain the age of the KLF. Whilst the use of the K-Ar and Ar-Ar methods to date the kimberlites and lamproites of southern India has been questioned (Kumar et al., 2007), studies elsewhere have successfully dated kimberlites and lamproites through applying the Ar-Ar dating technique to phlogopite (Phillips 1991), yielding ages which were consistent with previous age determinations using different methods. Lehmann et al. (2010) recently used the Ar-Ar age dating technique on phlogopite separates as well as U-Pb on perovskites to date kimberlites in the MKF, with both methods providing a similar age. We have also obtained new dates on some kimberlites from the EDC which agree with well-constrained published ages (Chalapathi Rao et al., 1999, Kumar et al., 2007). Comparison of our data with

previously published ages allows us to assess the reliability of our age data for the KLF.

### **3. Samples, methodology and analytical techniques**

#### *3.1 Samples analysed and assessment of alteration*

Samples were collected from the interior of each exposure (locations listed in Table 2). The kimberlites are classified as ‘Group I’ kimberlites on the basis of their mineralogy, in agreement with previous studies (e.g. Chalapathi Rao et al., 2004). Kimberlites and lamproites are susceptible to alteration processes and crustal contamination, and given the Proterozoic age of the rocks in this study, any interpretation of geochemical data must first consider the potential effect of these processes on the samples.

To assess any contamination or alteration effects, we first used the Ilmenite Index of Taylor et al. (1994), which identifies kimberlites and lamproites that may have accumulated or assimilated ilmenite megacrysts and xenocrysts. We also used loss on ignition (LOI) data as a proxy for alteration (Chalapathi Rao et al., 2004). Samples with high LOI are considered indicative of secondary alteration, commonly manifested in thin sections through increased abundances of secondary carbonate minerals and talc. Gd/Lu ratios of samples were also considered, where low values are indicative of HREE-enriched crustal contaminants (le Roex et al., 2003). A cut-off value of <58 was considered contaminated (Paton et al., 2009). The contamination index (CI, a measure of the proportions of clay minerals and tectosilicates relative to ferro-magnesian minerals - olivine, phlogopite) of Clement (1982) was used in this study, where a CI value of <1.5 is considered uncontaminated for kimberlites

(Mitchell, 1986). The kimberlite samples used in this study are below this cut-off value; however the lamproites show higher values, which are not unusual for such mica-rich rocks (Chalapathi Rao et al., 2004). CI values in the whole suite of samples from the Krishna lamproites ranged from 3.79-9.23.

Care was taken to ensure that all the samples we collected from the EDC were as fresh as possible. Those chosen for dating in this study are among the freshest and showed minimal contamination and alteration as identified by CI, LOI, Gd/Lu and Ilmenite Index determinations for our sample suite (Table 2).

### *3.2 Ar-Ar dating technique*

Age data for three samples are presented here, including two kimberlites (Mulgiripalle Pipe 5 and Tummatapalle pipe 13) from the WKF and one lamproite (Pochampalle) from the KLF. The Pochampalle lamproite is a NW-SE trending body located 2.5 km west of the Pochampalle village. Petrographic analysis of thin sections identified samples with the most suitable phlogopite grains for dating. The samples with freshest phlogopite were selected, with several samples discounted on the basis of high calcite content and alteration of phlogopite to chlorite. Once selected, microprobe analysis of phlogopite within each selected sample was used to determine the mineral chemistry.

Small blocks of each of the selected samples were then sawn, avoiding any crustal xenoliths, and crushed in a jaw crusher. The fragments were then sieved into fractions from which the phlogopite could be carefully picked (predominantly 300µm-500µm in length). The picked phlogopite grains were then washed in acetone using an

ultrasonic bath to remove any adhering material. The visibly fresh grains with fewest inclusions were then selected using a binocular microscope. These grains were then packaged in aluminium foil and sent for sample irradiation at McMaster University in Ontario, Canada. Irradiation flux was monitored using the GA1550 biotite standard with an age of  $98.79 \pm 0.54$  Ma (Renne et al., 1998). Sample J values were calculated by linear interpolation between two bracketing standards and are included in Table 3; a standard was included between every 8-10 samples in the irradiation tube. Blanks were measured either side of each measurement and used to correct each unknown, and  $^{37}\text{Ar}$  decay and neutron-induced interference reactions using the correction factors  $(^{39}\text{Ar}/^{37}\text{Ar})_{\text{Ca}} = 0.00065 \pm 0.000033$ ,  $(^{36}\text{Ar}/^{37}\text{Ar})_{\text{Ca}} = 0.000264 \pm 0.000013$  and  $(^{40}\text{Ar}/^{39}\text{Ar})_{\text{K}} = 0.0085$ , and the mass discrimination value used was 283. The decay constant of Steiger & Jäger (1977) was used.

Samples were loaded into an ultra-high-vacuum laser port and placed under a heat lamp for 8 hours to reduce atmospheric blank levels. Samples were analysed by total fusion of single grains using Nd-YAG 1064 nm infrared laser, or Nd-YAG 213 nm UV laserprobe, both coupled to a MAP 215-50 mass spectrometer. Gases were gettered for 5 minutes using two SAES getters one at 450°C and one at room temperature, and a liquid nitrogen cold trap, before inlet to the mass spectrometer. Peaks between  $^{35}\text{Ar}$  and  $^{41}\text{Ar}$  were scanned 10 times and amounts extrapolated back to the inlet time. Each analysis was background corrected using blank measurements bracketing every 1-2 samples.

The infrared-laser single-grain-fusion technique was applied to Muligiripalle Pipe 5 (Mul) and Tummatapalle pipe 13 (Tum) and Pochampalle (POCg) samples. Here

individual mineral grains were fused to yield a single age, and the final age is a weighted mean average, error and MSWD as calculated using Isoplot 3a (Ludwig, 2003) and reported at  $2\sigma$  level. The UV intragrain laserprobe technique was applied to POC and POCg samples, in which mineral grains were large enough to enable several measurements within each grain in order to test for heterogeneity (Figure 4.) (e.g., Kelley & Wartho, 2000; Sherlock et al., 2002). Each age determination was derived from a rastered laser pit measuring  $75\mu\text{m} \times 75\mu\text{m}$ , with a  $10\mu\text{m}$  diameter beam and reported at  $2\sigma$  level. In addition, grain margins were analysed using trenches parallel to the grain margins with a beam size of  $10\mu\text{m}$ . The number of analysis on each grain depended on its size, but can be seen in Figure 4. (The full dataset is available in online data repository where all values are reported in voltages)

### *3.3 Bulk-Rock and Isotopic measurements protocol*

1-2 kg of visibly unaltered kimberlite and lamproite samples were cut on a rock saw to remove any weathered portions and then reduced to small fragments in a jaw-crusher. These fragments were then crushed to powder in an agate ring mill to produce the powders used in all bulk-rock geochemical analysis.

Two methods were used to obtain bulk-rock major-, trace- and REE data. Major and some minor elements (Al, Ca, Fe, K, Mg, Mn, Na, P, Si, Ti, Ba, Cr, Ni, Sr, Y, Zr), were analysed using Inductively-Coupled Plasma Atomic Emission Spectroscopy (ICP-AES). 100 mg of powdered sample was fused with 300 mg  $\text{LiBO}_2$  (lithium metaborate) flux, and then dissolved in dilute  $\text{HNO}_3$ . The concentrations of selected major- and trace-elements were then determined by ICP-AES at the Natural History Museum, London. These solutions were not spiked. Reference materials were selected

based on their similarities to the samples to be analysed and included BCR-1 (major and trace) and GA (trace and REE).

HF/HClO<sub>4</sub> (hydrofluoric acid/perchloric acid) digestion was used for other minor-, trace- and REE analyses. In each case, 500 mg of powdered sample underwent a total digestion in HF/HClO<sub>4</sub>. The resulting solution was evaporated to dryness, and the residue was then dissolved in dilute nitric acid. The concentrations of trace-elements were then determined by ICP-AES and ICP-MS, as required, at the Natural History Museum, London. Solutions for ICP-MS were diluted a further 10 times and were spiked with 1 ppb In and 1 ppb Rh as internal standards prior to analysis. ICP-AES solutions were not spiked. To monitor instrumental drift and precision the standard BCR-1 was used. Major, trace and REE element analysis were found to be better than  $\pm 20\%$  (2 s.d.) to that of the certified values, with the exception of Ni, Cr, Sn and Be which were found to be better than  $\pm 30\%$  (2 s.d.) to that of the certified values and Bi, Cd, and Ta which showed slightly greater deviation to that of certified values.

The four dated samples underwent Nd isotope analysis. 50 mg of powdered sample was weighed in each case and spiked with a <sup>150</sup>Nd/<sup>144</sup>Nd solution. These samples underwent a total digestion in HF/HNO<sub>3</sub>. Nd and Sm were separated from the dissolved samples by standard ion-exchange techniques (Cohen et al., 1988), using cation columns to collect the REE fraction, which was then passed through HDEHP columns to collect Nd and Sm fractions, which were evaporated to dryness. 1 µl of 2M HCl was added to the Nd collected for each sample and then loaded with 0.6 µl of 0.01M H<sub>3</sub>PO<sub>4</sub> onto the centre of an outgassed Re filament. Nd isotopic ratios were measured in the static mode using a Triton thermal ionization mass spectrometer at

the Open University. Reproducibility of the La Jolla Nd standard over the analysis period was  $0.511849 \pm 0.000002147$  (8 ppm, 2SD)

## **4. Results**

### *4.1 Ar-Ar dating*

The Ar-Ar dating results are summarised in Table 3 and reported to  $2\sigma$ . Where infrared laserprobe analysis is performed on mineral separates each age is derived from the total fusion of an individual mineral grain.

#### *4.1.1 Kimberlites: Muligiripalle Pipe 5 and Tummatapalle Pipe 13*

For the Muligiripalle Pipe these ages range from  $1088 \pm 5$  to  $1149 \pm 21$  Ma ( $n=18$ ) with a weighted mean age of  $1113 \pm 3$  Ma (MSWD=0.96;  $n=17$ ). For the Tummatapalle Pipe the age range from  $1098 \pm 16$  to  $1138 \pm 29$  Ma ( $n=10$ ), with a weighted mean age of  $1105 \pm 12$  (MSWD=0.24;  $n=10$ ).

#### *4.1.2 Lamproite: Pochampalle*

Infrared laserprobe analysis yields individual mineral ages in the range  $1408 \pm 5$  to  $1614 \pm 8$  Ma ( $n=6$ ). With such a scatter in age data it is important to assess the spatial variation of ages within individual mineral grains which is achievable using the ultraviolet intra-grain technique. Five different mineral grains from two samples have been analysed using this technique (Figure 4). From sample POC ages within the internal parts of the mineral grains range from  $1543 \pm 39$  to  $1611 \pm 32$  Ma, and from the grain margins range from  $1480 \pm 35$  to  $1625 \pm 15$  Ma ( $n=8$ ). From sample POCg ages within the internal parts of the mineral grains range from  $1463 \pm 71$  to  $1684 \pm 100$  Ma ( $n=24$ ) and from the grain margins range from  $1507 \pm 38$  Ma to  $1698 \pm 30$  Ma ( $n=11$ ).



382

## 383 4.2 Geochemistry

### 384 4.2.1 Geochemical and isotopic data on the Krishna lamproites

385 Major, trace and REE data were obtained on lamproites from 9 different locations (the  
386 full dataset is available in the online data repository). Two samples were analysed  
387 from two of the lamproites, Vedadri (VEDN and VEDS) and Pochampalle (POC and  
388 POCg); in each case, the two samples were collected from different locations within  
389 the same lamproite body. 8 of the lamproite samples are from the KLF, while one  
390 (Chelima) is located within the Cuddapah Basin (Table 2).

391

392 All of the lamproites in this study are LREE enriched, as shown by elevated  $(La/Yb)_N$   
393 values (Figure 5). For the Krishna lamproites,  $(La/Yb)_N = \sim 45$  to 75. The  
394 Pochampalle lamproite shows even greater LREE enrichment compared to the rest of  
395 the KLF samples with  $(La/Yb)_N = \sim 100$ . The Chelima lamproite has the highest  
396 degree of LREE enrichment among the sample suite analyzed in the present study,  
397 with  $(La/Yb)_N = \sim 200$ . These values are comparable to other published ratios for the  
398 KLF  $(La/Yb)_N = 51-173$  (Chalapathi Rao et al., 2010) and Chelima  $(La/Yb)_N = 72-$   
399 247 (Chalapathi Rao et al., 2004).

400

401 On a chondrite-normalized REE plot (Figure 6), all lamproites from the EDC display  
402 similar LREE-enriched patterns. The Chelima lamproite shows the steepest REE  
403 pattern. Two samples were collected from different locations from the Pochampalle  
404 lamproite and show slightly different REE patterns (Fig 6). The POC sample shows a  
405 trend closer to those of the KLF, especially for the HREE, though with a higher La/Yb  
406 ratio due to greater LREE enrichment. The POCg sample has an even higher La/Yb

ratio due to its extreme LREE enrichment (similar to that of Chelima), but has higher HREE contents than Chelima. The HREE enrichment may be due to variations in the source but can also be attributed to crustal contamination. However, even if the samples have undergone some degree of crustal contamination, it is unlikely to have affected the isotopic ratios of small-fraction melts, because the concentrations of Sm and Nd in crustal rocks is likely to be much lower than in the kimberlitic melts (e.g. Fraser et al., 1985; Gibson et al., 1996).

The Pochampalle ( $^{143}\text{Nd}/^{144}\text{Nd(m)} = 0.511059$ ) and Chelima ( $^{143}\text{Nd}/^{144}\text{Nd(m)} = 0.511129$ ) lamproites also show lower Nd isotopic values than the rest of the lamproites in the KLF ( $^{143}\text{Nd}/^{144}\text{Nd(m)} = 0.511348\text{--}0.511459$ ) (Figure 7). In contrast to the REE data, the  $^{143}\text{Nd}/^{144}\text{Nd}$  isotopic ratio of Pochampalle is not intermediate between that of Chelima and the Krishna lamproite group.

The lower  $^{143}\text{Nd}/^{144}\text{Nd}$  ratio of the Pochampalle lamproite suggests a closer affinity with the CLF, particularly Chelima, than with the rest of the KLF samples. The broad spread of the KLF Nd data precludes robust interpretations of a mixing array involving the Cuddapah Basin Lamproites (CBL), Pochampalle and the Krishna lamproites. However, the difference in Nd isotopic signature between Pochampalle and the other Krishna lamproites is striking.

The Nd evolution through time of the southern Indian kimberlites and lamproites in this study is summarised in Figure 8, and compared with model evolution curves for depleted mantle (DM; Workman and Hart, 2005), and enriched mantle (EM). The enriched mantle is modelled using the  $\epsilon\text{Nd}$  value of a garnet lherzolite xenolith from

the Lattavaram kimberlite in the EDC (Karmalkar et al. 2009), and assuming a representative value of  $^{143}\text{Nd}/^{144}\text{Nd}$  for enriched mantle (EMI; Hart et al., 1992).

The  $\epsilon\text{Nd}$  evolution trajectory of the kimberlites intersects the  $\text{EM}^*_x$  model evolution line at around 1 Ga, which corresponds to the emplacement age of the EDC kimberlites. However, the DM and  $\text{EM}^*_x$  model evolution lines intersect much earlier (1.9-2.0 Ga). One model for petrogenesis of the EDC kimberlites consistent with these Nd evolution data is that the kimberlite magmas were derived at around 1 Ga from an initially depleted mantle source that had been enriched at around 1.9-2 Ga.

The mantle source from which the lamproites were derived is not tightly constrained by the evolution curves in Figure 8. Their enriched geochemistry indicates that they did not originate directly from a depleted mantle source, but clearly they have a different source to that of the kimberlites. It is also apparent that the Pochampalle and Chelima lamproites followed a separate evolution from the other Krishna lamproites.

It is possible that Pochampalle and Chelima lamproites were derived from a different source altogether from other Krishna lamproites. However, they may have been derived from the same source as the Krishna lamproites but at an earlier time. This source could have been an ancient depleted mantle that was enriched prior to lamproite generation. More definite conclusions are difficult to draw from Nd evolution modelling of the lamproites due to the isotopic heterogeneity of the sub-continental lithospheric mantle, even on relatively small length scales.

## 5. Discussion

Despite the recent increase in scientific interest in the kimberlites and lamproites of the Dharwar Craton in southern India, the ages of the kimberlites and in particular lamproites are poorly constrained. An age of around 1.1 Ga for both the kimberlites in the WKF and NKF appears to be well supported, although many pipes within these fields are yet to be dated. The only lamproite previously dated from the KLF is the Ramannapeta lamproite, even though there are many lamproites in the KLF; and it would seem presumptuous to assume an age for the entire field based on one age from one lamproite. However, this age has been used in several studies to represent an age for the KLF mainly because of a lack of any other reliable age data (Reddy et al., 2003, Paul et al., 2007, Chakrabarti et al., 2007)

The Ar-Ar ages for Muligiripalle of  $1113 \pm 3$  Ma and for Tummatapalle of  $1105 \pm 12$  are consistent with previous age determinations for the WKF and in particular Muligiripalle, which has been dated at  $1093 \pm 20$  (Kumar et al., 1993) by Rb-Sr technique and  $1153 \pm 17$  (Chalapathi Rao., 1996) by K-Ar technique. The Pochampalle lamproite from the KLF yields a much older age than the published K-Ar and Rb-Sr age dates for the KLF ( $1224 \pm 14$  Ma on the Ramannapeta lamproite; Kumar et al., 2001). However, both the K-Ar and Rb-Sr ages were described as tentative by the authors as they were unable to rule out the effects of excess extensive secondary carbonation (Rb-Sr) and the possibility of excess Ar in mantle-derived phlogopite (K-Ar). We dated samples from two different locations from within the Pochampalle lamproite (POCg and POC). The dating of kimberlites and lamproites has been the subject of discussion, because in many cases phlogopite cores are older than their rims, which is true of the Pochampalle lamproite. In rocks formed and cooled in mid- and upper-crustal settings this is usually attributed to either prolonged

482 cooling imparting an ‘age’ gradient or partial resetting of a mineral and argon-loss  
483 occurring at the rims (e.g. Sherlock et al., 2002). In kimberlites and lamproites the  
484 same observed age patterns are argued to be due to a pervasive and uniformly-  
485 distributed excess argon component derived from a deep fluid source (e.g. Phillips &  
486 Onstott, 1988; Phillips 1991; Phillips et al., 1999) that is then partially outgassed to  
487 the grain boundary network during incorporation into the magma chamber (Pearson et  
488 al., 1997). Phillips & Onstott (1988) compared step-heating spectra of two sets of  
489 phlogopite mineral separates with *in situ* data obtained from a single large phlogopite  
490 grain using a continuous wave infrared Nd-YAG laser. The step-heating spectra  
491 identify the range of ages preserved within the mineral separates but without  
492 identifying the spatial distribution of the ages, whilst the laserprobe data identifies the  
493 position of the ages within the grain. The resolution of the laserprobe data is limited  
494 by the area outside the point of laser-sample interaction that is outgassed due to heat  
495 conduction during lasing; Phillips & Onstott (1988) report a resolution of 80-150µm  
496 diameter pits separated by distances of 20-100µm, which gave sufficient confidence  
497 that the individual age measurements were not affected by adjacent laser pits. The age  
498 range of ca. 1200 to ca. 1540 Ma from low- to high-temperature steps in the heating  
499 spectra indicate a range of ca. 1200 Ma to ca. 2200 Ma (Phillips & Onstott, 1988), the  
500 oldest age represented by a single laser spot. The differences were difficult to  
501 reconcile but it was considered that the old ages could be ‘masked’ during physical  
502 mineral decrepitation during step-heating and the mixing of different aged reservoirs  
503 within the mineral separates. Notably, the volume of phlogopite preserving old  
504 apparent ages is a small fraction of the grain and so it is conceivable that during the  
505 preparation of the mineral separates by crushing and sieving this low-volume  
506 component might not be well represented. The study raised more questions about the

behaviour of argon in such high pressure and high temperature minerals. Phillips (1991) also compared step-heating and laserprobe Ar-Ar data, and analysed matrix and macrocryst phlogopites. The former yielded plateau ages that were consistent with eruption ages and the latter yielded complex release patterns concurring with those reported by Phillips & Onstott (1988). In contrast the laserprobe data (spatial resolution of 100x200µm sized pits in the internal parts of the grain and up to 160x400µm at the rim, separated by 30-80µm) reveal older cores and younger rims, with similar conclusions to Phillips & Onstott (1988), in that a high concentration of excess argon was trapped in the macrocrysts prior to eruption, the rims record the eruption age, and the matrix phlogopites record the eruption age (Phillips, 1991). This model dictates that radiogenic argon is retained in minerals in the upper mantle at temperatures of 700°C or more (Pearson et al., 1997). Kelley & Wartho (2000) were able to test this by analysing well-characterised xenoliths from two different settings, with robust age constraints, using the high spatial resolution ultra-violet laserprobe approach to assess core-rim age differences in detail. The results showed old cores and young rims, and in both settings the older core ages corresponded to magmatic/metasomatic events that were recorded by other isotope systems (Kelley & Wartho, 2000). The rims were also younger than the cores, with argon-loss profiles of 200 to 300µm in length decreasing to the known eruption age at the grain edge (Kelley & Wartho, 2000). This study identified that the phlogopites retained argon at temperatures hundreds of degrees higher than the phlogopite closure temperature (ca. 450° C) and that argon loss at the grain margins represents the integrated time-temperature history as the xenolith travels from depth to emplacement at the surface (Kelley & Wartho, 2000). The key difference between this study and the conclusions of Phillips et al (1991; 1999) is in the interpretation of the core-rim age differences:

Phillips (1991) and Phillips et al (1999) interpret old cores due to excess argon whilst Kelley & Wartho (2000) interpret them as retained radiogenic argon because of a lack of transfer of argon to the grain boundary network because the grains behave as 'closed systems' under the high pressures experienced in the mantle and lower crust.

In terms of our new data for the Pochampalle lamproite, macrocrystic phlogopite yielded single grain fusion ages that spanned ca. 200 Myr, and the intra-grain ultraviolet laserprobe analysis revealed a complex age structure with older internal parts and varied rim ages. Individually the five grains are different, in size and shape, but the age ranges for each of the grains are very similar, most notably for sample POC. Contouring is not appropriate in this case because there are two analytical approaches – ablating squares in internal parts of the grains and margin-parallel trenches – and taking the approach of plotting age versus distance from the centre of the laser pit to the nearest grain margin can reveal information on the age structure (Figure 9).

Sample POC preserves cores of ca 1560 Ma to ca 1610 Ma with a single data point that is much higher (ca. 1660 Ma). In both grains the measurements actually at the grain margins are the youngest – ca. 1500 Ma and ca. 1480 Ma. In POCg the same age pattern is observed though with more scatter, and the key point is that in plotting data in this way it assumes that the distance from laser pit to grain margin now, is the same as it was at the time of mineral growth, a likely false assumption given the difficulty in recovering intact mineral grains. Notably for POCg the grain margins are consistently the youngest with ages of ca 1493 Ma, ca. 1463 Ma and ca. 1507 Ma, although there is notable scatter in the third grain from sample POCg in which two grain margins are measured, one of which is significantly older than the other and

may not represent an original grain margin. The internal parts of the grain are consistently in the range ca. 1530 Ma to ca. 1630 Ma. The key points to note are: 1) in five mineral grains from samples POC and POCg the grain margins are the youngest parts of the grains and are all within error of 1500 Ma; 2) the internal parts of the mineral grains are significantly older and in the region of ca. 1550-1650 Ma. These observations are in keeping with those of Phillips & Onstott (1988), Phillips (1991), Phillips et al (1999) and Kelley & Wartho (2000). Whether the older core regions of the minerals reflect excess argon or retention of radiogenic argon under mantle-lower crust conditions is difficult to discern, but by and large this is a moot point. It is the ages recorded by the rims of the minerals that are of importance since these are considered to represent the timing of eruption by all the previously cited studies.

To summarise the new Ar-Ar data, ages from the two kimberlite pipes derived from matrix phlogopites are consistent and yield an age of ca. 1100 Ma for their eruption. The Pochampalle lamproite preserves old ages in internal parts of the grain that could be due to either excess argon retention or quantitative retention of radiogenic argon, whilst the rims record an eruption age of ca. 1500 Ma.

Based on these Ar-Ar age data, we propose that the Pochampalle lamproite was emplaced ~1500 Ma ago, roughly 250 Myr before the rest of the KLF. It would seem that the Pochampalle magma was also derived from an isotopically distinct mantle source from the rest of the KLF lamproites with a lower  $^{143}\text{Nd}/^{144}\text{Nd}$  ratio. Trace element geochemistry implies that it may have been derived by relatively smaller degrees of partial melting from within the garnet stability field compared to the rest of the KLF. The Nd isotopic signature and the bulk-rock REE pattern in the Pochampalle



lamproite appear to be consistent with a hypothesis that a heterogeneous mantle source was sampled by the Krishna lamproites during the Proterozoic.

Insight into the possible tectonic setting for emplacement of the Pochampalle lamproite could come from recent work by Hou et al. (2008). Citing a giant radiating dyke swarm and LIPs at ~1.85 Ga, they propose that the North China Craton, Indian Craton and Canadian Shield were united together in a single landmass before its extension and break-up. The Mesoproterozoic Belt–Purcell–Uinta rift system (1470–1440 Ma) (Sears et al., 1998) along the west margin of the Canadian Shield suggests that the North China Craton and the Indian Craton were ultimately separated from the Laurentia continent by around 1.5 Ga onwards. This is close to the emplacement age of the Pochampalle lamproite, which could therefore be linked to this period of continental rifting.

The older age and smaller degrees of mantle partial melting inferred for the Pochampalle lamproite may correspond to initiation of lithospheric stretching beneath the southern Indian craton at ~1500 Ma. The continuation or pre-existence of such a weakness in the lithosphere may have been exploited by later emplacement of the Krishna lamproites, by which time the mantle source region had acquired modified isotopic signatures through melt percolation from the asthenospheric mantle.

Previously, the Chelima lamproite (ca. 1400 Ma) was thought to be one of the oldest recorded lamproites in the world (Chalapathi Rao, 2007). However, our age data suggest that at least one lamproite (Pochampalle) was generated in the same region 100 Ma before the Chelima lamproite. This not only has implications for regional

ultramafic magmatism, but also demonstrates that the mantle mechanism for producing lamproitic melts existed earlier than previously thought. It seems likely that further age determinations on Indian lamproites may extend their age range even further.

### **Acknowledgements**

IO acknowledges a NERC PhD studentship NE/F008805/1 with NHM CASE support. IO and MA would like to thank N.V. Chalapathi Rao for facilitating the field trip and his help in sample collection.

### **References**

- Anand, M., Gibson, S.A., Subbarao, K.V., Kelley, S.P., and Dickin, A.P., 2003. Early Proterozoic Melt Generation Processes beneath the Intra-cratonic Cuddapah Basin, Southern India: *Journal of Petrology*, v. 44, p.2139-2171.
- Anders, E., and Grevesse, N., 1988. Abundances of the elements: Meteoritic and solar: *Geochimica et Cosmochimica Acta*, v. 53, p.197-214.
- Chakrabarti, R., Basu, A.R., and Paul, D.K., 2007. Nd-Hf-Sr-Pb isotopes and trace element geochemistry of Proterozoic lamproites from southern India: Subducted komatiite in the source: *Chemical Geology*, v. 236, p. 291-302.
- Chalapathi Rao, N.V., Miller, J.A., Pyle, D.M., Madhavan, V., 1996. New Proterozoic K-Ar ages for some kimberlites and lamproites from the Cuddapah Basin and Dharwar Craton, South India: evidence for non-contemporaneous emplacement: *Precambrian Research*, v. 79, p. 363-369.
- Chalapathi Rao, N.V., Miller, J.A., Gibson, S.A., Pyle, D.M., and Madhavan, V., 1999. Precise  $^{40}\text{Ar}/^{39}\text{Ar}$  age determinations of the Kotakonda kimberlite and the Chelima lamproite, India: Implication to the timing of mafic dyke swarm emplacement in the Eastern Dharwar Craton: *Journal of the Geological Society of India*, v. 53, p. 425-432.
- Chalapathi Rao, N.V., Gibson, S.A., Pyle, D.M., and Dickin, A.P., 2004. Petrogenesis of Proterozoic Lamproites and Kimberlites from the Cuddapah Basin and Dharwar Craton, Southern India: *Journal of Petrology*, v. 45, p. 907-948.
- Clement, C.R., 1982. A comparative geological study of some major kimberlite pipes in northern Cape and Orange Free State: Ph.D. thesis, University of Cape Town.
- Cohen, A.S., O'Nions, R. K., Siegenthaler, R. & Griffin, W. L., 1988. Chronology of the pressure-temperature history recorded by a granulite terrain: *Contributions to Mineralogy and Petrology*, v. 98, p. 303-311.

- Davies, G.R., Stolz, A.J., Mahotkin, I.L., Nowell, G.M., Pearson, D.G., 2006. Trace element and Sr–Pb–Nd–Hf isotope evidence for ancient, fluid-dominated enrichment of the source of Aldan Shield lamproites: *Journal of Petrology*, v. 47, p. 1119-1146.
- Dalziel, I.W.D., Mosher, S., Gahagan, L.M., 2000. Laurentia-Kalahari Collision and the Assembly of Rodinia: *The Journal of Geology*, v. 108, p. 499-513.
- Ernst, R.E., Buchan, K.L., 2001. Large mafic magmatic events through time and links to mantle-plume heads, *in* Ernst, R.E., Buchan, K.L., ed., *Mantle Plumes: Their Identification Through Time*. Geological Survey of America Special Paper, Volume 352, p. 483-575.
- Gopalan, K., and Kumar, A., 2008. Phlogopite K-Ca dating of Narayanpet kimberlites, south India: Implications to the discordance between their Rb-Sr and Ar-Ar ages: *Precambrian Research*, v. 167, p. 377-382.
- Hanson, R.E., Crowley, J.L., Bowring, S.A., Ramezani, J., Gose, W.A., Dalziel, I.W.D., Pancake, J.A., Seidel, E.K., Blenkinson, T.G., Mukwakwami, J., 2004. Coeval large-scale magmatism in the Kalahari and Laurentian cratons during Rodinia assembly: *Science*, v. 304, p. 1126-1129.
- Hart, S.R., Hauri, E.H., Oschmann, L.A., and Whitehead, J.A., 1992. Mantle plumes and entrainment—Isotopic evidence: *Science*, v. 256, p. 517-520.
- Heaman, L.M., Kjarsgaard, B.A., Creaser, R.A., 2003. The timing of kimberlite magmatism in North America: implications for global kimberlite genesis and diamond exploration: *Lithos*, v. 71, p. 153-184.
- Hou, G., Santosh, M., Qian, X., Lister, G.S., Li, J., 2008. Configuration of the Late Paleoproterozoic supercontinent Columbia: Insights from radiating mafic dyke swarms: *Gondwana Research*, v. 14, p. 395-409.
- Karmalkar, N.R., Duraiswami, R.A., Chelapathi Rao, N.V., Paul, D.K., 2009. Mantle-derived Mafic-ultramafic Xenoliths and the Nature of Indian Sub-continental Lithosphere: *Journal of the Geological Society of India*, v. 73, p. 657-679.
- Kelley, S.P., and Wartho, J.A., 2000. Rapid kimberlite ascent and the significance of Ar-Ar ages in xenolith phlogopites: *Science*, v. 289.
- Kumar, A., Kumari, P., Dayal, A.M., Murthy, D.S.N., and Gopalan, K., 1993. Rb-Sr ages of Proterozoic kimberlites of India: evidence for contemporaneous emplacement: *Precambrian Research*, v. 62, p. 227-237.
- Kumar, A., and Gopalan, K., Rao, K.R.P., and Nayak, S.S., 2001. Rb-Sr Age of kimberlites and lamproites from Eastern Dharwar Craton, South India: *Journal of the Geological Society of India*, v. 58, p. 135-141.
- Kumar, A., and Gopalan, K., 2005. Comments on: 'Petrogenesis of Proterozoic Lamproites and Kimberlites from the Cuddapah Basin and Dharwar Craton, Southern India: *Journal of Petrology*, v. 46, p. 1077-1079.

- Kumar, A., Heaman, L.M., Manikyamba, C., 2007. Mesoproterozoic kimberlites in south India: A possible link to ~1.1Ga global magmatism: *Precambrian Research*, v. 154, p. 192-204.
- Lehmann, B., Burgess, R., Frei, D., Belyatsky, B., Mainkar, D., Chalapathi Rao, N.V., Heaman, L.M., 2010. Diamondiferous kimberlites in central India synchronous with Deccan flood basalts: *Earth and Planetary Science Letters*, v. 290, p. 142-149.
- Ludwig, K.R., 2003. *ISOPLOT 3.00: A Geochronological Toolkit for Microsoft Excel* Berkeley Geochronology Center, Berkeley, California.
- Mitchell, R.H., 1986. *Kimberlites: Mineralogy, Geochemistry, and Petrology*: New York, Plenum Press, 442 p.
- Murphy, D.T., Collerson, K. D., Kamber, B. S., 2002, Lamproites from Gaussberg, Antarctica: possible transition zone melts of Archaean subducted sediments: *Journal of Petrology*, v. 43, p. 981-1001.
- Nagaraja Rao, B.K., Rajurkar, S. T., Ramalingaswamy, G., Ravindra Babu, B., 1987. Stratigraphy, structure and evolution of the Cuddapah Basin: *Geological Society of India Memoir*, v. 6, p. 33-86.
- Paton, C., Hergt, J.M., Woodhead, J.D., Phillips, D., Shee, S.R., 2009. Identifying the asthenospheric component of kimberlite magmas from the Dharwar Craton, India: *Lithos*, v. 112, p. 296-310.
- Paul, D.K., Crocket, J.H., Reddy, T.A.K., and Pant, N.C., 2007. Petrology and geochemistry including Platinum Group Element abundances of the Mesoproterozoic ultramafic (lamproite) rocks of Krishna District, southern India: Implications for source rock characteristics and petrogenesis: *Journal of the Geological Society of India*, v. 69, p. 577-596.
- Peslier, A.H., Woodland, A.B., and Wolff, J.A., 2008. Fast kimberlite ascent rates estimated from hydrogen diffusion profiles in xenolithic mantle olivines from southern Africa: *Geochimica Cosmochimica Acta*, v. 72, p. 2711-2722.
- Pearson, D.G., Kelley S.P., Pokhilenko, N.P., and Boyd, F.R., 1997. Laser  $^{40}\text{Ar}/^{39}\text{Ar}$  analyses of phlogopites from Southern African and Siberian kimberlites and their xenoliths: Constraints on eruption ages, melt degassing and mantle volatile compositions: *Russian Journal of Geology and Geophysics*, v. 38, p. 106-117.
- Phillips, D., 1991. Argon isotope and halogen chemistry of phlogopite from South African kimberlites: a combined step-heating, laser probe, electron microprobe and TEM study: *Chemical Geology (Isotope Geoscience Section)*, v. 87, p. 71-98.
- Phillips, D., and Onstott, T.C., 1988, Argon isotopic zoning in mantle phlogopite: *Geology*, v. 16, p. 542-546.

- 752 Phillips, D., Kiviets, G.B., Barton, E.S., Smith, C.B., Viljoen, K.S., and Fourie, L.F.,  
753 1999.  $^{40}\text{Ar}/^{39}\text{Ar}$  dating of kimberlites and related rocks: problems and solutions: 7<sup>th</sup>  
754 International Kimberlite Conference (Cape Town), v.2, p. 677-688.  
755
- 756 Reddy, T.A.K., Sridhar, M., Ravi, S., Chakravarthi, V., Neelakantam, S., 2003.  
757 Petrography and geochemistry of the Krishna lamproite field, Andhra Pradesh:  
758 Journal of the Geological Society of India, v. 61, p. 131-146.  
759
- 760 Renne, P.R., Swisher, C.C., Deino, A.L., Karner, D.B., Owens, T.L., DePaolo, D.J.,  
761 1998. Intercalibration of standards, absolute ages and uncertainties in  $^{40}\text{Ar}/^{39}\text{Ar}$   
762 dating: Chemical Geology, v. 145, p. 117-152.  
763
- 764 Sears, J.W., Chamberlain, K.R., Buckley, S.N., 1998. Structural and U–Pb  
765 geochronologic evidence for 1.47 Ga rifting event in the Belt basin, western Montana:  
766 Canadian Journal of Earth Sciences, v. 35, p. 467-475.  
767
- 768 Sherlock, S., Kelley, S., 2002. Excess argon evolution in HP–LT rocks: a UVLAMP  
769 study of phengite and K-free minerals, NW Turkey: Chemical Geology, v. 182, p.  
770 619-636.  
771
- 772 Sherlock, S.C., Jones, K.A., and Kelley, S.P., 2002. Fingerprinting polyorogenic  
773 detritus using the  $^{40}\text{Ar}/^{39}\text{Ar}$  UV laserprobe: Geology, v. 30, p. 515-518.  
774
- 775 Skinner, E.M.W., Smith, C.B., Bristow, J.B., Scott Smith, B.H., and Dawson, J.B.,  
776 1985. Proterozoic kimberlites and lamproites and a preliminary age for the Argyle  
777 lamproite pipe, Western Australia: Geological Society of South Africa v. 88, p. 335-  
778 340.  
779
- 780 Steiger, R.H., Jager, E., 1977. Subcommision on geochronology: Convention on the  
781 use of decay constants in geo- and cosmochemistry: Earth and Planetary Science  
782 Letters, p. 359-362.  
783
- 784 Taylor, W.R., Tompkins, L. A., Haggerty, S. E., 1994. Comparative geochemistry of  
785 West African kimberlites: evidence for a micaceous kimberlite end member of sub-  
786 lithospheric origin: Geochimica Cosmochimica Acta, v. 58, p. 4017-4037.  
787
- 788 Workman, R.K., Hart, S.R., 2005. Major and trace element composition of the  
789 depleted MORB mantle (DMM): Earth and Planetary Science Letters, v. 231, p. 53-  
790 72.  
791  
792

## Figure Captions

**Figure 1.** Location of the Krishna lamproites relative to the major tectonic domains of southern India. HKF: Hinota Kimberlite Field; MKF: Mainpur Kimberlite Field; NKF: Naryanpet Kimberlite Field; WKF: Wajrakarur Kimberlite Field. Modified from Paton et al. (2009)

**Figure 2.** Location and extent of kimberlite and lamproite fields around the Cuddapah Basin, showing the locations of individual pipes. Modified from Chalapathi Rao et al. (2009). The inset shows the location of the KLF expanding north to provide a more detailed map of the Krishna lamproite field (KLF) showing the location of the individual lamproite pipes including Pochampalle (KLP on diagram). Modified from Chakrabarti et al. (2007).

**Figure 3.** Typical microtextures of phlogopite in the analysed samples. Each set shows a back-scattered electron image (left) and an element map for potassium (right). a) Muligiripalle kimberlite (pipe 5, WKF), scale bars 200  $\mu\text{m}$ ; b) Tummatapalle kimberlite (pipe 13, WKF), scale bars 100  $\mu\text{m}$ ; c) Pochampalle lamproite (KLF), scale bars 500  $\mu\text{m}$ .

**Figure 4.** Sketches of phlogopite grains analysed using UV intragrain laserprobe technique. Each age determination was derived from a rastered laser pit measuring 75  $\mu\text{m}$  x 75  $\mu\text{m}$ , with a 10  $\mu\text{m}$  diameter beam. The number of analyses on each grain depended on its size.

**Figure 5.** Plot of Dy/Yb against La/Yb (normalized to chondrite; values from Anders and Grevesse, 1988) for the Krishna lamproites and Chelima lamproite. Data from Chak (Chakrabarti et al., 2007) and Chal (Chalapathi Rao et al., 2004) are also shown.

**Figure 6.** Chondrite-normalized (values from Anders and Grevesse, 1988) REE plot for the Krishna lamproites (average abundance), the Chelima lamproite (solid line), and the two Pochampalle lamproite samples (dashed lines).

**Figure 7.** Plot of  $1/[\text{Nd}]$  against  $^{143}\text{Nd}/^{144}\text{Nd}$  ratios for the Krishna lamproites (including Pochampalle) and the CLF (including Chelima). Data are from this study, Chakrabarti et al. (2007) (Chak) and Chalapathi Rao et al. (2004) (Chal).

**Figure 8.** Plot of  $\epsilon\text{Nd}$  against time for the lamproites (solid lines) from the EDC (data from this study). The Pochampalle and Chelima lamproites are shown as bolder solid lines. Also shown is the range of kimberlites data from the EDC (shaded field; Paton et al., 2009). The single bold dashed line represents the potential Nd evolution of enriched mantle ( $\text{EM}^*_x$ ) beneath India, modelled using the  $\epsilon\text{Nd}$  of a garnet lherzolite xenolith from the Lattavaram kimberlite in the EDC (Karmalkar et al. 2009), combined with a representative value of  $^{143}\text{Nd}/^{144}\text{Nd}$  for EMI (Hart et al., 1992). The depleted mantle (DM) trend (dotted line) uses data from Workman and Hart (2005).

**Figure 9.** Age versus distance from grain edge for all UV laserprobe data points from phlogopite macrocrysts from: a) Sample POC; b) Sample POCg.

**Table 1.** Compilation of dates obtained on kimberlites and lamproites from the Eastern Dharwar Craton and related areas

Date (Ma)	Method	Material	Samples <sup>2</sup>	Field	Authors <sup>2</sup>
<b>Wajrakurur Kimberlite Field (WKF)</b>					
1093 ±20	Rb-Sr	phlogopite	Muligiripalle pipe 5	WKF	K et al. 93
1153 ±17	K-Ar	phlogopite	Muligiripalle pipe 5	WKF	CR et al. 96
1091 ±20	Rb-Sr	phlogopite	Wajrakarur pipe 1	WKF	K et al. 93
1092 ±15	Rb-Sr	phlogopite	Wajrakarur pipe 2	WKF	K et al. 93
1102 ±23	Rb-Sr	phlogopite	Wajrakarur	WKF	K et al. 07
1124 ±5	U-Pb	perovskite	Wajrakarur	WKF	K et al. 07
1091 ±10	Rb-Sr	phlogopite	Venkatampalle pipe 7	WKF	K et al. 93
<b>Narayanpet Kimberlite Field (NKF)</b>					
1363 ±48	K-Ar	phlogopite	Kotakonda	NKF	CR et al. 96
1401 ±5	Ar-Ar	phlogopite	Kotakonda	NKF	CR et al. 99
1085 ±14	Rb-Sr	phlogopite	Kotakonda	NKF	K et al. 01
1099 ±12	Rb-Sr	phlogopite	Mudalabad	NKF	K et al. 01
1167 ±86	K-Ca	phlogopite	Narayanpet	NKF	G & K 08
1093 ±4	Rb-Sr	phlogopite	Siddanpalle	NKF (SKF)	K et al. 07
1063 ±41	K-Ca	phlogopite	Siddanpalle	NKF (SKF)	G & K 08
<b>Mainpur Kimberlite Field (MKF)</b>					
60 – 65	Ar-Ar & U-Pb	Phlogopite & Perovskites	Behradih Kodomali	MKF (~700 km N)	L et al. 2010
<b>Hinota Kimberlite Field (KKF)</b>					
1067 ±31	Rb-Sr	phlogopite	<i>Majhgawan</i>	HKF (1000 km N)	K et al. 93
<b>Cuddapah Basin Lamproites (CB)</b>					
1350 ±52	K-Ar	phlogopite	<i>Chelima</i>	CB	CR et al. 96
1418 ±8	Ar-Ar	phlogopite	<i>Chelima</i>	CB	CR et al.

					99
1354 ±17	Rb-Sr	phlogopite	<i>Chelima</i>	CB	K et al. 01
1090	Rb-Sr	phlogopite	<i>Zangamarajupall e</i>	CB	K et al. 01
<b>Krishna Lamproite Field (KLF)</b>					
1384 ±18	K-Ar	phlogopite	<i>Ramannapeta</i>	KLF	CR et al. 96
1224 ±14	Rb-Sr	phlogopite	<i>Ramannapeta</i>	KLF	K et al. 01

<sup>1</sup> Kimberlites: plain type; *lamproites: italics*.

<sup>2</sup> K et al. 93: Kumar et al. (1993); CR et al. 96: Chalapathi Rao et al. (1996); CR et al. 99: Chalapathi Rao et al. (1999); K et al. 01: Kumar et al. (2001); K et al 07: Kumar et al. (2007); G & K 08: Gopalan and Kumar (2008); L et al., 2010: Lehmann et al. (2010).



**Table 2.** Location and Contamination/Alteration of Samples.

Name	Longitude (degrees N)	Latitude (degrees E)	CI	LOI % Wt Loss	Ilmenite Index	Gd/Lu
Muligiripalle (K)	14° 85' 74''	77 ° 32' 06''	1.34	6.24	0.59	74.50
Tummatapalle (K)	14 ° 84' 55''	77 ° 30' 09''	1.19	8.62	0.67	80.64
Pochampalle (L)	16 ° 83' 79''	80 ° 16' 61''	5.09	3.91	1.23	92.69
Pochampalle G (L)	16 ° 84' 59''	80 ° 16' 38''	4.41	3.40	0.62	74.44

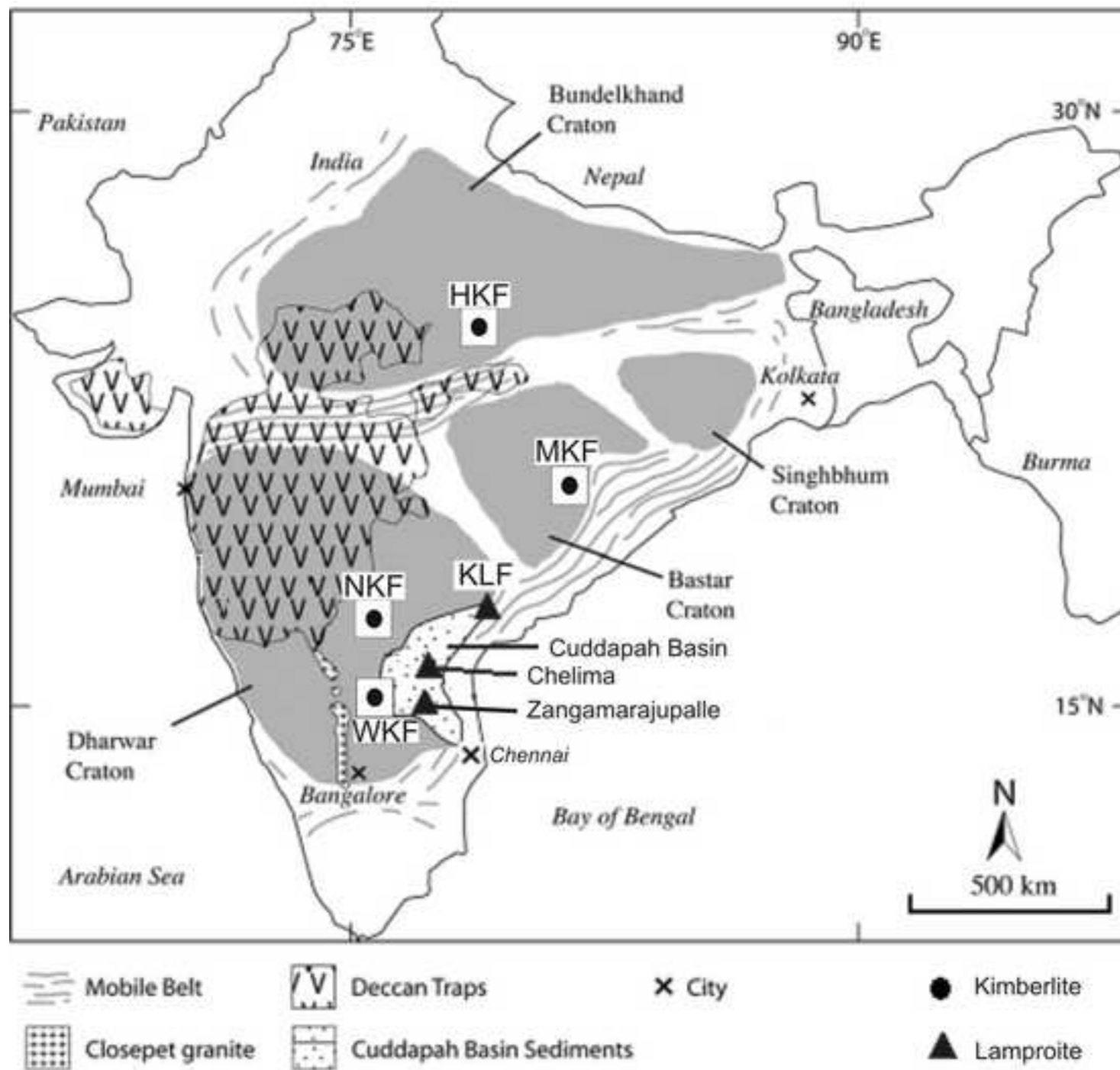
**Table 3.** Ar-Ar results.

Sample	Rock Type	Method <sup>1</sup>	Wtd Mean (Ma)	Error (±)	MSWD	Number of analyses
Muligiripalle	Kimberlite	TF	1109	6	2.7	12 grains fused
Muligiripalle	Kimberlite	TF	1115	4	0.78	6 grains fused
Tummatapalle	Kimberlite	TF	1105	12	0.24	10 grains fused
Pochampalle	Lamproite	UV	1575	20	1.3	14 points on single grain (Fig. 4a)
Pochampalle	Lamproite	UV	1568	55	11.3	6 points on single grain (Fig. 4b)
Pochampalle	Lamproite	TF	1523	110	16.3	6 grains fused
Pochampalle G	Lamproite	UV	1563	25	6.8	12 points on single grain (Fig. 4c)
Pochampalle G	Lamproite	UV	1564	51	0.52	8 points on single grain (Fig. 4d)
Pochampalle G	Lamproite	UV	1583	16	2.5	15 points on single grain (Fig. 4e)

<sup>1</sup> TF = Total fusion analysis; UV = Ultraviolet laser *in situ* analysis

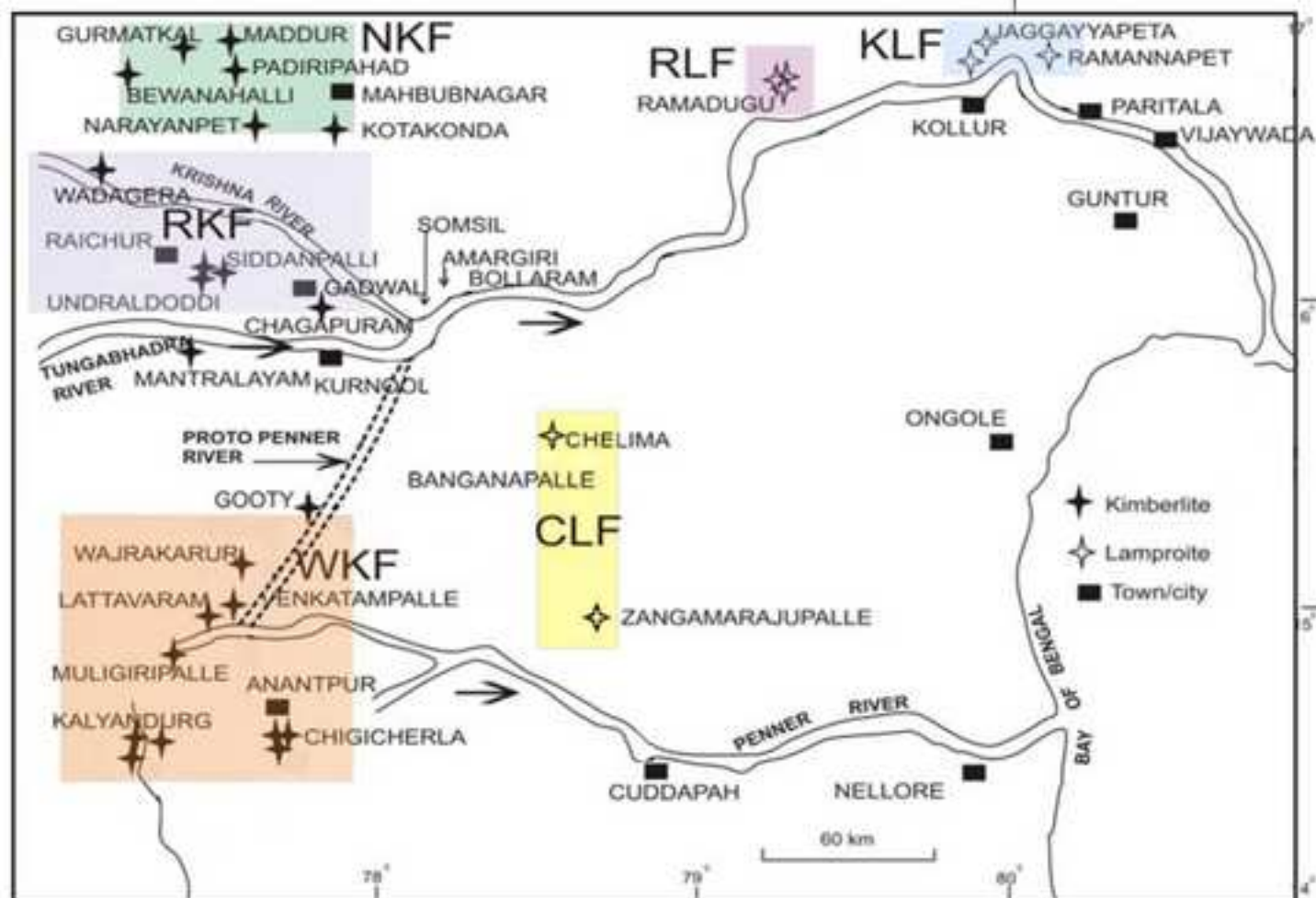
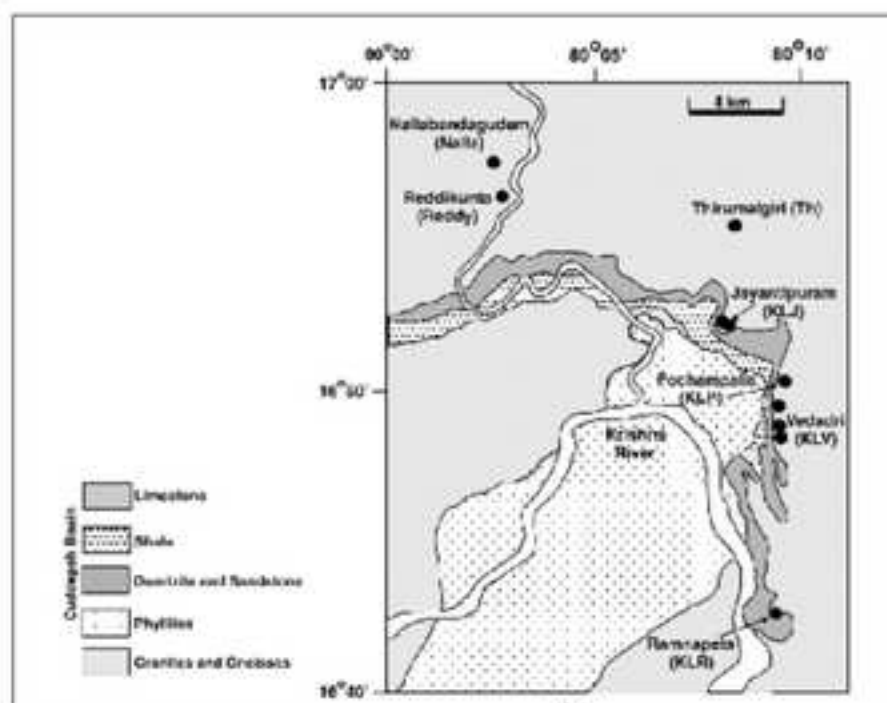
Figure

[Click here to download high resolution image](#)



Figure

[Click here to download high resolution image](#)



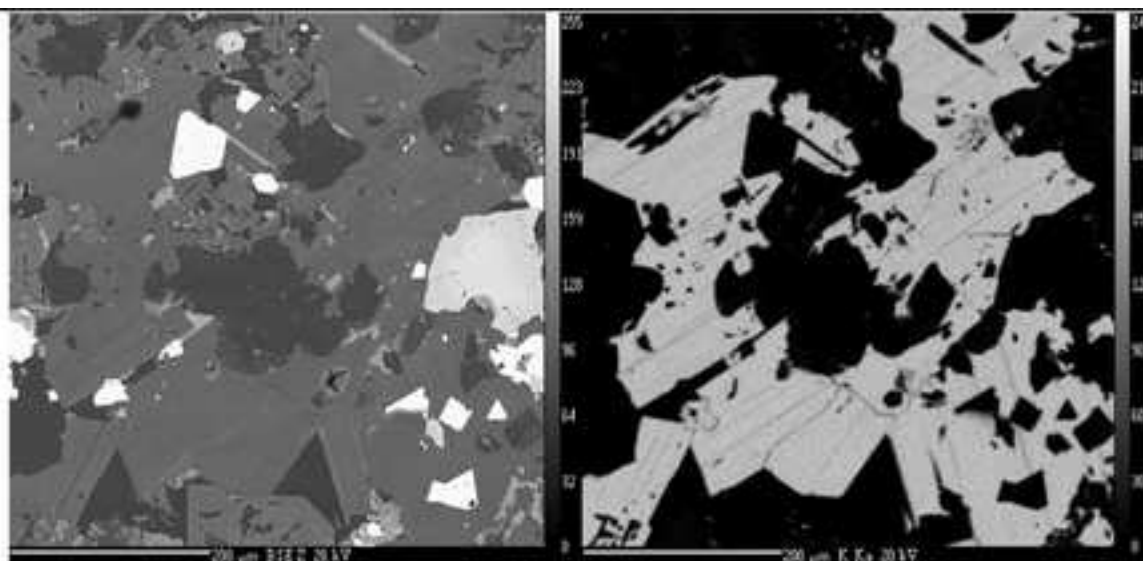


Fig 3a

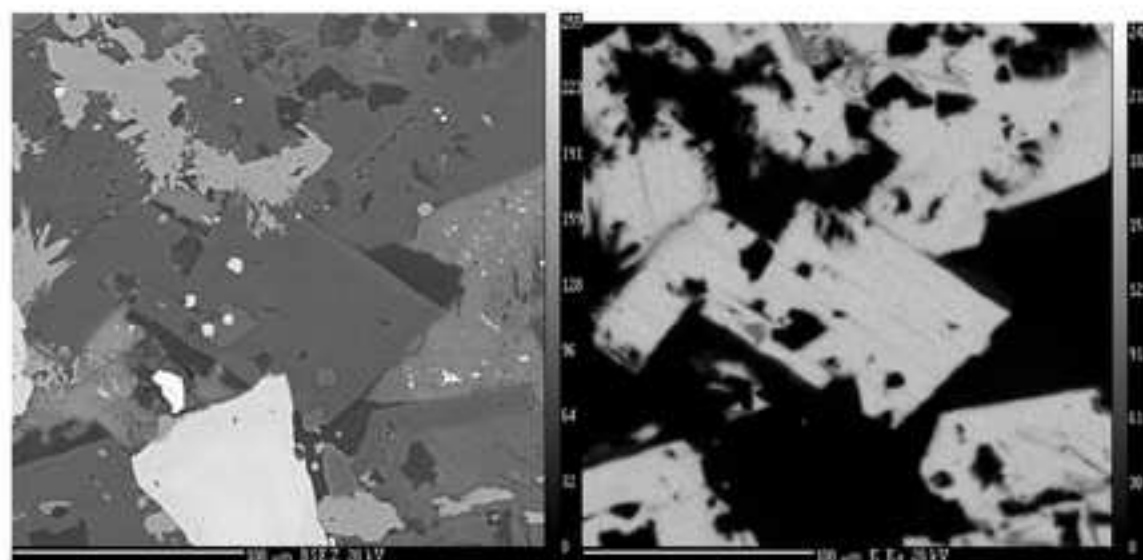


Fig 3b

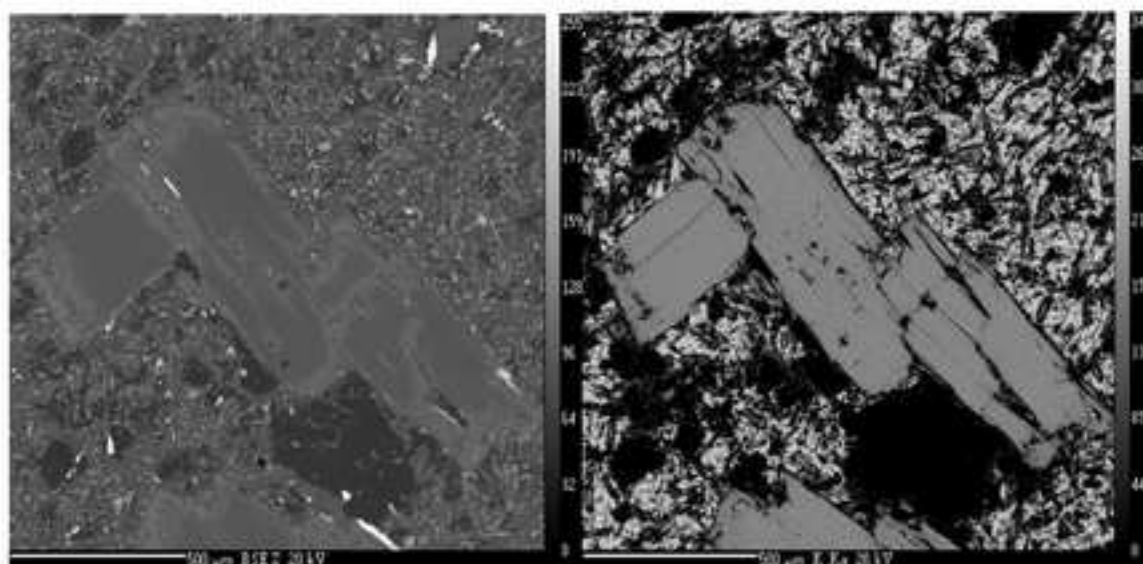


Fig 3c

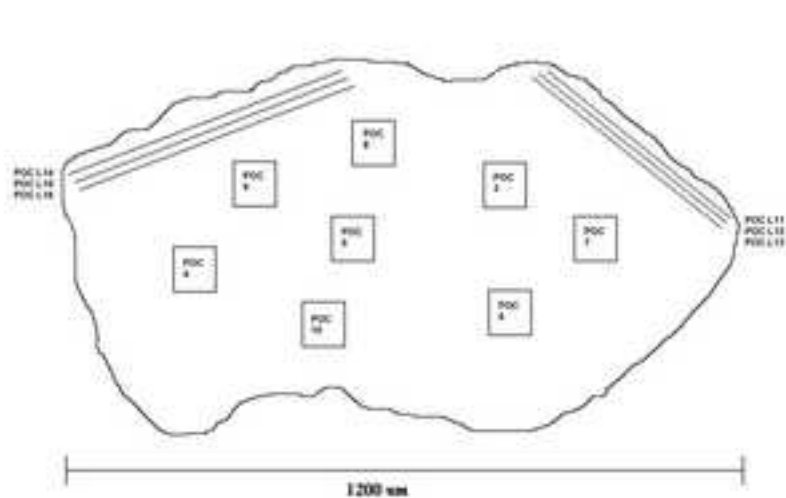


Fig. 4 POC analysis

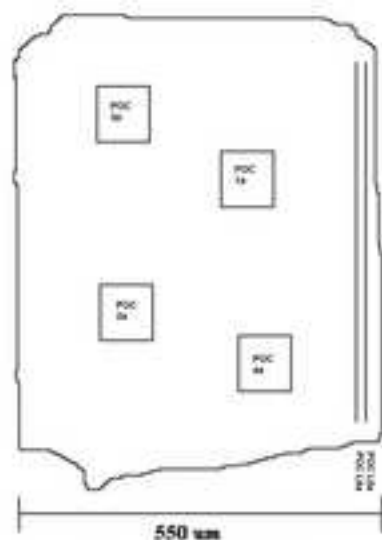


Fig. 4a POC analysis

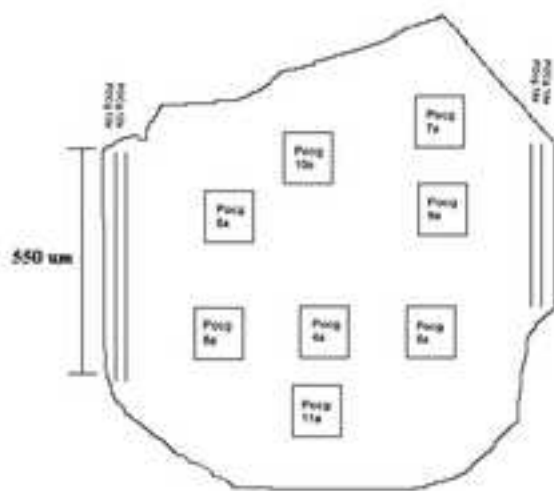


Fig. 4b POCg analysis

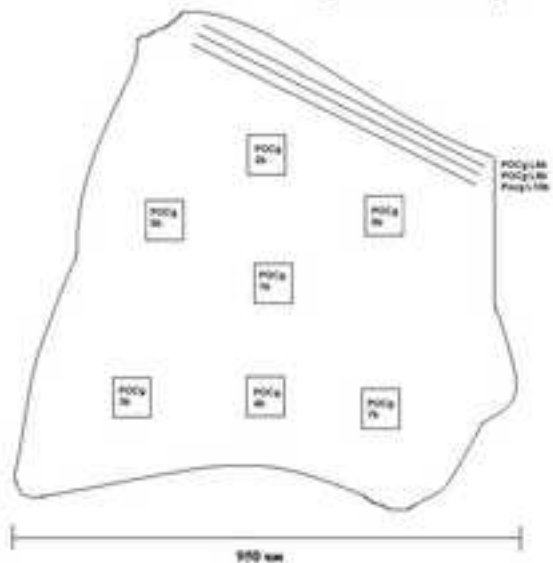


Fig. 4c POCg analysis

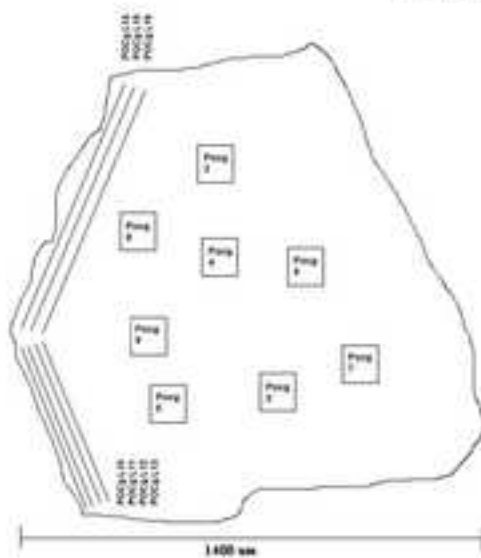


Fig. 4d POCg analysis

Figure

[Click here to download high resolution image](#)

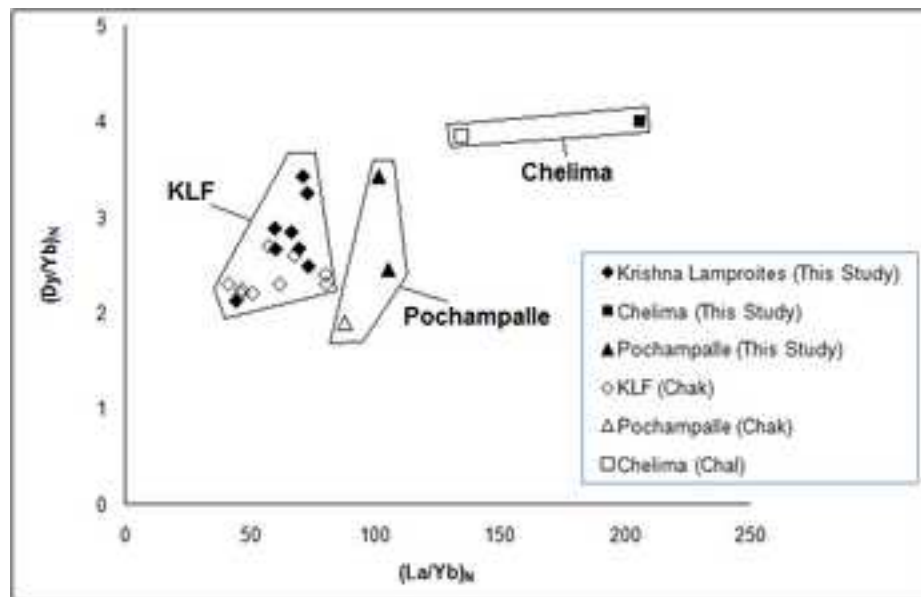
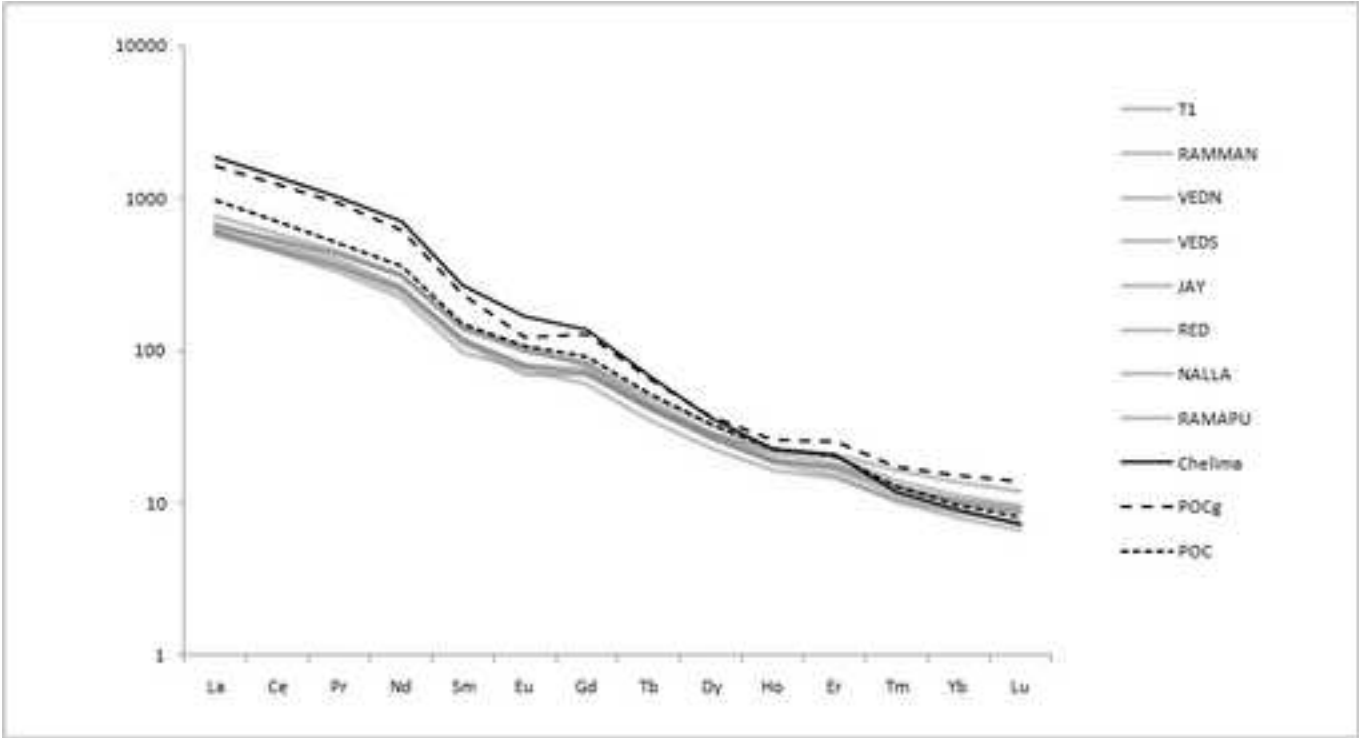




Figure  
[Click here to download high resolution image](#)





Figure

[Click here to download high resolution image](#)

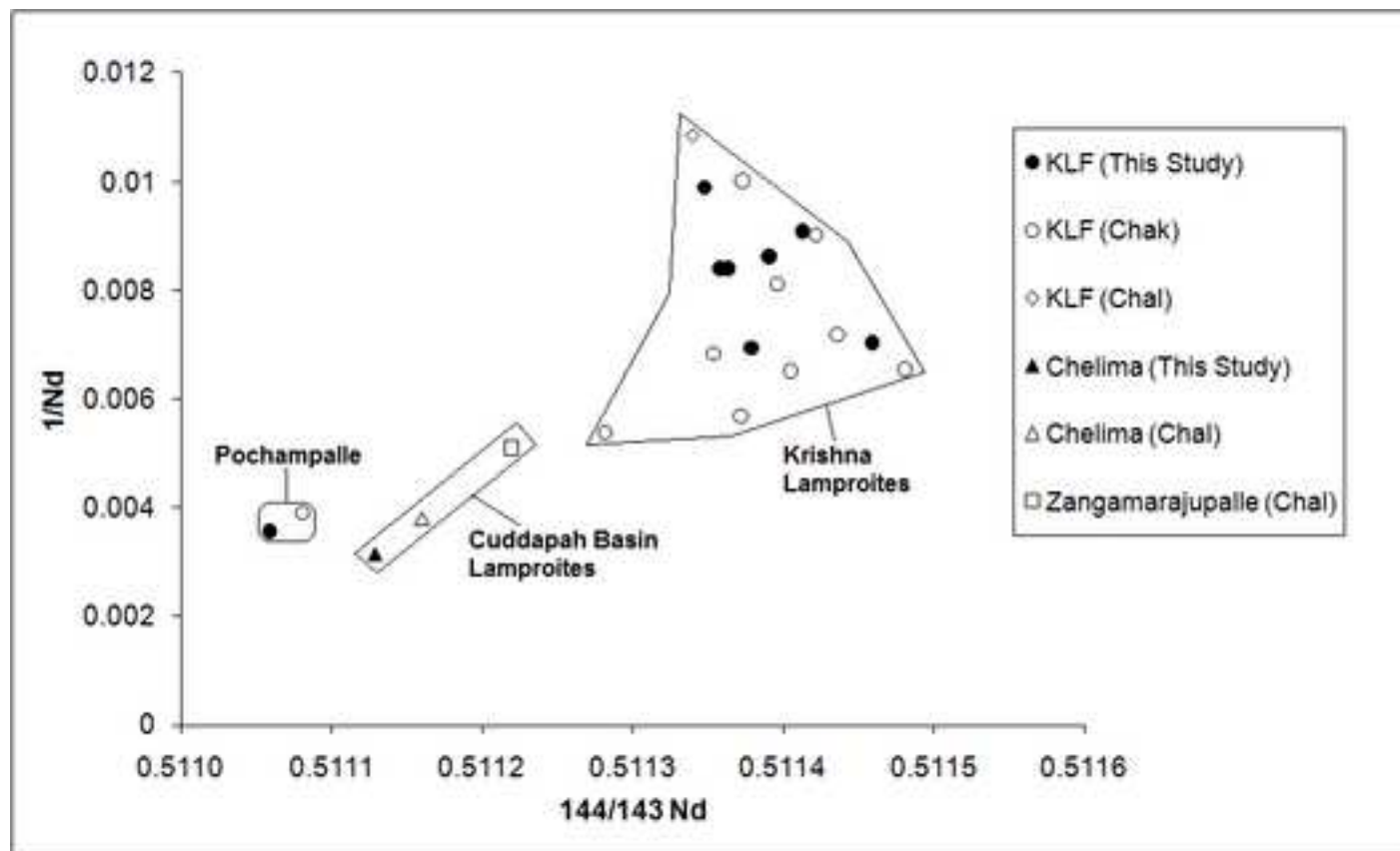
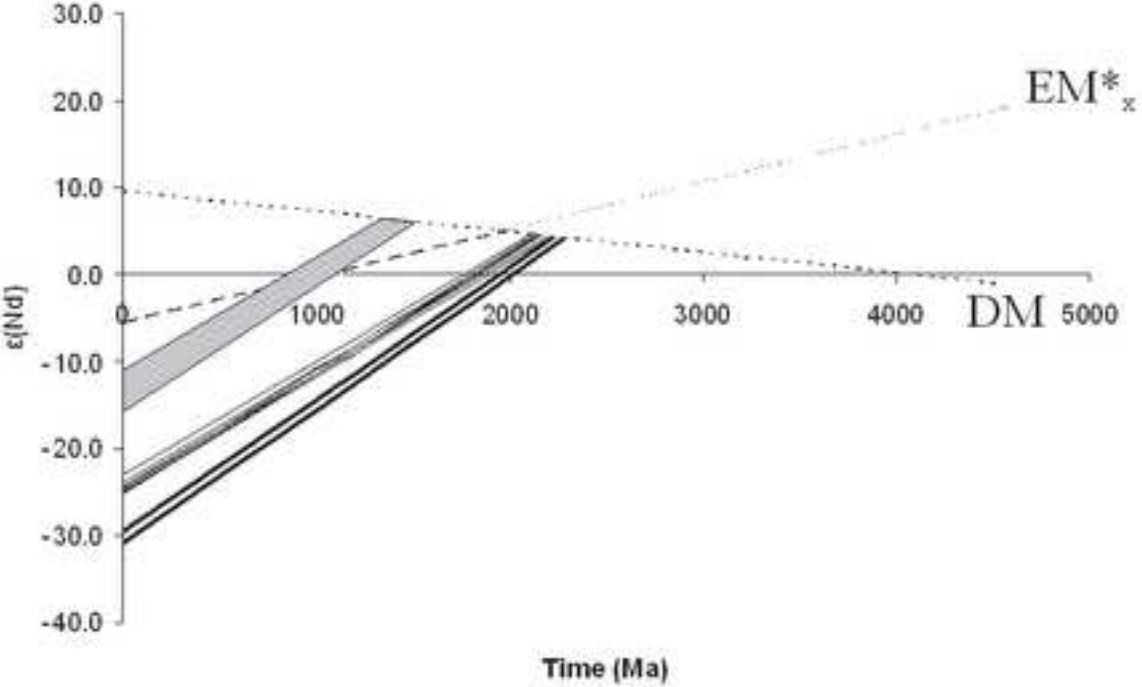
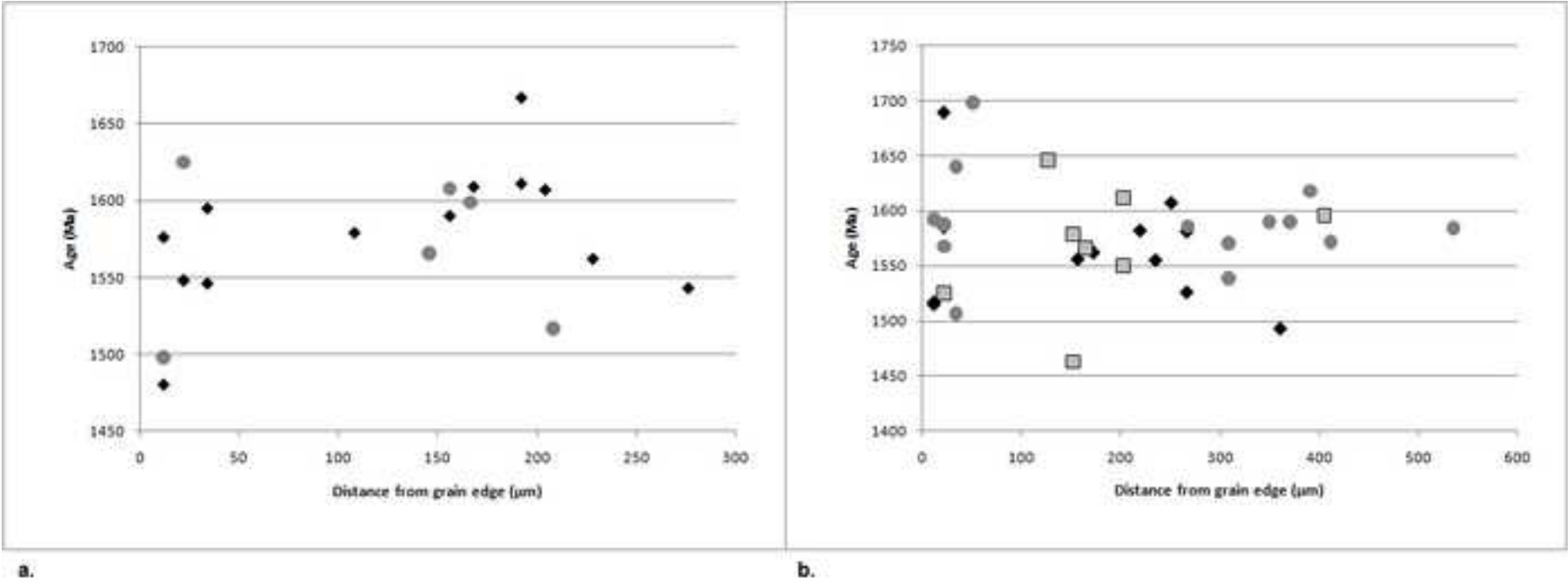


Figure  
[Click here to download high resolution image](#)



Figure

[Click here to download high resolution image](#)



Supplementary material for on-line publication

[Click here to download Supplementary material for on-line publication: Ar Data for publication 2010.xls](#)

Supplementary material for on-line publication

[Click here to download Supplementary material for on-line publication: Nd Data for publication.xls](#)

Supplementary material for on-line publication

[Click here to download Supplementary material for on-line publication: WR Data for publication.xls](#)